Highly Dispersed Zn Sites on ZrO_2 by Flame Spray Pyrolysis for CO_2 Hydrogenation to methanol

By

Kakeru Fujiwara[1*], Taiki Akutsu[1], Masahiko Nishijima[2], Shohei Tada[3*],

1. Department of Chemistry and Chemical Engineering, Yamagata University, 4–3-6 Jonan, Yonezawa, Yamagata 992–8510, Japan

2. Flexible 3D System Integration Laboratory, Sanken, Osaka University, 8–1 Mihogaoka, Ibaraki, Osaka 567-0047 Japan

3. Division of Applied Chemistry, Faculty of Engineering, Hokkaido University, N13 W8, Kita-Ku, Sapporo, Hokkaido 060-8628, Japan

Submitted to

Topics in Catalysis

for the special issue for Waste-to-Value Towards Green and Circular Economy,

Kakeru Fujiwara: k_fujiwara@yz.yamagata-u.ac.jp

Shohei Tada: shohei.tada.st@eng.hokudai.ac.jp

Abstract

In this study, we synthesized *x*ZnO-ZrO_2 (*x* = 14-40 at%) by flame spray pyrolysis under a lean-fuel condition. The optimal ZnO content was investigated to obtain a ZnO-ZrO_2 solid solution with high specific surface area for CO_2-to-methanol hydrogenation. The Zn species in ZnO-ZrO_2 were highly dispersed and hexagonal ZnO was not detected by X-ray diffraction (XRD). After heating the particles in Ar at 400 °C for 3 h, hexagonal ZnO particles were observed at *x* = 40 at%, while below *x* = 28 at%, the Zn species remained high dispersion state. A fraction of the Zn species was substituted into the bulk of the ZrO_2 particles, as evidenced by the shift of the ZrO_2 (101) peak in the XRD patterns. The elemental mapping of Zn and Zr in 28 at% ZnO-ZrO_2 showed that the Zn species on the surface were uniformly distributed. The presence of partially reduced $Zr^{\delta+}$ state ($\delta < 4$) was confirmed by X-ray photoelectron spectroscopy. The $Zr^{\delta+}$ state in the ZnO-ZrO_2 particles was prominent when ZnO content was below 28 at%. The catalytic activity of 28 at% ZnO-ZrO_2 for CO_2-to-methanol hydrogenation was higher than that of 40 at% ZnO-ZrO_2. At 300 °C and 1.0 MPa, the CO_2 conversion and the selectivity to methanol over 28 at% ZnO-ZrO_2 were 9% and 48%, respectively, resulting in the high yield of methanol (4.3%).

Keywords: Methanol synthesis, Flame synthesis, solid solution, Zn substitution, tetragonal ZrO_2

Graphical abstract

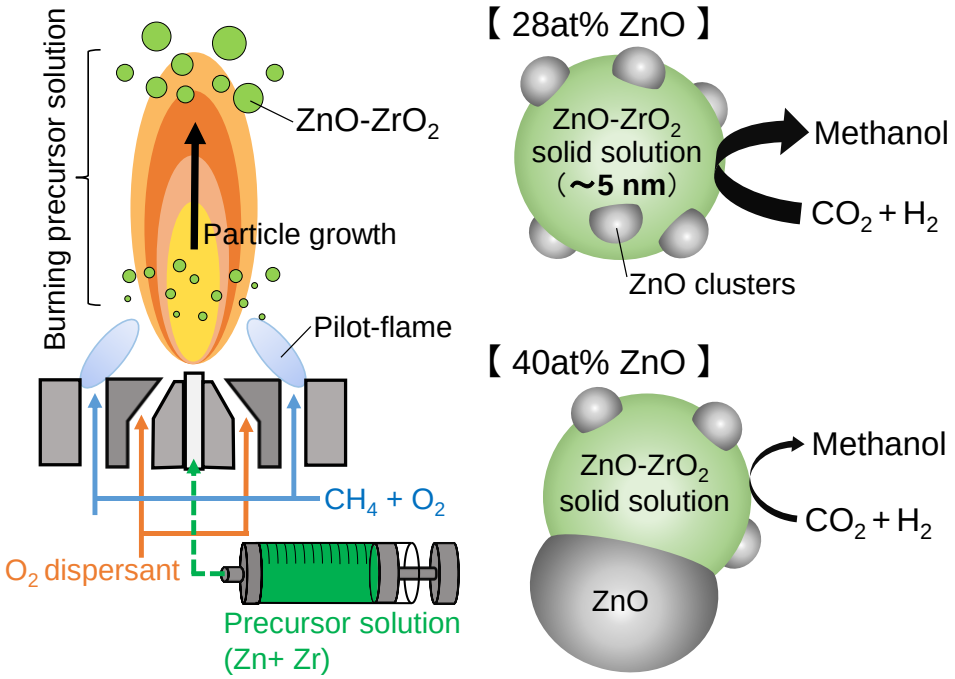

1. Introduction

Alternatives to finite fossil resources have long been sought. Methanol obtained via the hydrogenation of CO_2 with H_2 generated by renewable energy is one of the candidates because it can be used as a liquid fuel and feedstock for many chemicals. [1] When methanol is further transformed into a feedstock (e.g., light olefins), a methanol-to-olefins (MTO) reaction is required. Thus, to produce feedstock from CO_2, two reactors are necessary for CO_2-to-methanol hydrogenation and the MTO reaction, which results in high energy consumption. To address this issue, bifunctional catalysts have attracted much attention. The bifunctional catalyst contains two types of catalysts for CO_2 hydrogenation to methanol and MTO reactions.

Many catalysts for CO_2 hydrogenation to methanol have been developed, such as Cu- [2-9], In- [10, 11], Pd- [12-14], and alloys- [15-17] based catalysts, but these are aimed to improve the catalytic performance at relatively low temperatures (~250 °C). Since the MTO reaction typically takes place above 300 °C, a CO_2 hydrogenation catalyst that is effective above that temperature is desired. For the CO_2 hydrogenation above 300 °C, Wang et al. proposed ZnO-ZrO_2 as a promising candidate. [18] They also investigated the catalytic activity of metal oxides combined with ZrO_2 and found that Zn-, Ga-, and Cd-oxides were promising. [19] Tada et al. [20] discovered that ZnO-ZrO_2 showed the highest methanol production rate above 275 °C among MO_x-ZrO_2 (*M*: Zn, Mn, Cu, Al, Ga, and In). In these catalysts, the existence of a ZnO-ZrO_2 solid solution accounts for their high performances because Zn-O-Zr sites play an essential role. [18, 19, 21] Tada et al.[22] revealed that the Zn-O-Zr sites of the solid solution are more active compared to the ZnO surface sites and interfacial sites between ZnO and ZrO_2. So far, many studies on ZnO-ZrO_2 solid solution catalysts have been reported. Li et al. [23] used a metal−organic framework as a precursor for the solid solution. Han et al. [24] applied evaporation-induced self-assembly method to synthesize the solid solution with ordered mesoporous structure. However, the specific surface area (SSA) of the reported catalysts is relatively small (44-139 $m^2\ g^{-1}$) [18, 20, 21, 23, 24], and there is room for improvement.

To obtain a solid solution with a high SSA, flame spray pyrolysis (FSP) will be promising. [25] FSP can be scaled up to kg h^{-1} of a production rate and used in industries. [26] In FSP, metal precursors are sprayed into droplets and combusted to generate metal oxide particles. The particles are formed in high-temperature flame with a very short residence time, producing small particles. [27, 28] Rapid quenching at high temperatures allows the formation

of unique solid solutions, such as $Ce_{1-x}Zr_xO_2$ [29], Ti-substituted ZnO [30], Pd-substituted TiO_2 [31], and (Mn-Fe-Ni-Cu-Zn)$_3O_4$ [32]. In addition, FSP can deposit atomically dispersed VO_x [33], Cu [34], Pd [31, 35], and Pt [36] on metal oxides which demonstrate superior catalytic performance. Šot et al. [37] synthesized highly dispersed ZnO on ZrO_2 by FSP and demonstrated its high activity for CO_2 hydrogenation. However, the SSA of the catalysts (63-89 $m^2 g^{-1}$) was comparable to that of the catalysts synthesized by other methods (44-139 $m^2 g^{-1}$) [18, 20, 21, 23, 24]. Furthermore, they could not obtain a ZnO-ZrO_2 solid solution using FSP. Štefanić et al. [38] observed the segregation of Zn^{2+} species from ZrO_2 above 600~700 °C. Thus, even if a solid solution initially forms in a flame, the high temperature of the flame facilitates the segregation of Zn species from ZrO_2. To minimize the segregation, the residence time of the particles in the flame should be reduced. The residence time can be decreased by decreasing the length and temperature of the flame. [39]

In this study, we synthesized *x*ZnO-ZrO_2 (*x* = 14-40 at%) using FSP under a lean-fuel condition. Such condition produced a relatively cold and short flame to minimize the segregation of Zn^{2+} species from ZrO_2. The optimal ZnO content was explored to obtain a ZnO-ZrO_2 solid solution with high SSA. Powder X-ray diffraction (PXRD), X-ray photoelectron spectroscopy (XPS), scanning transmission electron microscopy (STEM), and N_2 adsorption were performed to identify the optimal ZnO content. The catalytic performance of FSP-made ZnO-ZrO_2 for CO_2 hydrogenation to methanol was evaluated and compared to the performance of ZnO-ZrO_2 catalysts reported in literature.

2. Experimental

2.1 Catalyst preparation

ZnO-ZrO_2 catalysts and reference samples (ZrO_2 and ZnO) were prepared by combusting the precursor solution in an FSP reactor [25]. An appropriate amount of zirconium isopropoxide solution (70 wt% in 1-propanol, TCI) was added to 2-ethyl hexanoic acid (2-EHA; Sigma-Aldrich, purity > 99%). After stirring the solution for 2 min, methanol (MeOH; Fujifilm Wako Pure Chemical, Guaranteed Reagent Grade) was added in 2-EHA: MeOH ratio of 1:1 (in vol.) and, subsequently, zinc acetylacetonate (Kanto Chemical) was dissolved in the

solution. The ZnO content was adjusted by controlling the Zn/Zr ratio in the solution, and the concentration of metals (Zn + Zr) was fixed at 0.2 mol L^{-1}.

The precursor solution was fed into the reactor at 2 mL min^{-1} and atomized by O_2 dispersant (8 L min^{-1}), as shown in Fig. 1. The dispersed precursor droplets were ignited by a pilot-flame (CH_4 and O_2 at 1.5 and 3.2 L min^{-1}, respectively). The combustion of the precursor resulted in the formation of ZnO-ZrO_2 particles, which were collected by a vacuum pump (Seco SV1040, Busch) and a glass fiber filter (Albet LabScience, GF6, 257 mm in diameter). The distance between the FSP nozzle and filter was set at 65 cm. As required, the particles were treated with Ar at 400 °C for 3 h.

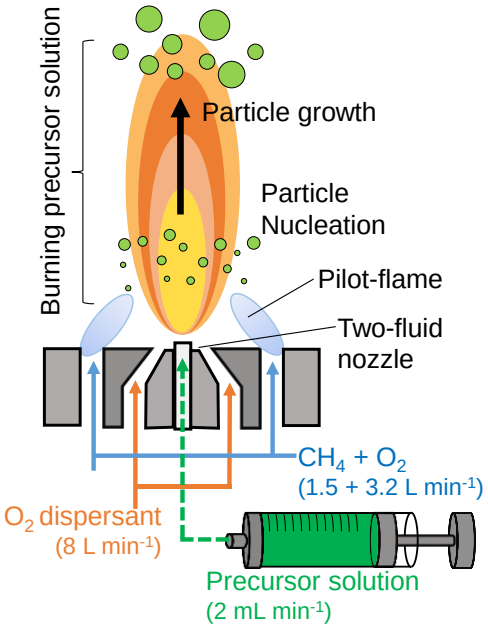

Fig. 1 Schematic of particle production by an FSP reactor.

2.2 Catalyst characterization

Powder X-ray diffraction (PXRD) was performed using a diffractometer (Rigaku, Miniflex, Cu Kα, 40 kV, 15 mA). The crystallite size of t-ZrO_2 and the lattice spacing of the (101) plane were calculated from the peak at 30° using Scherrer's equation (Eq. (1)) and Bragg's equation (Eq. (2)), respectively.

$$d_{\mathrm{XRD}}\ [\mathrm{nm}] = \frac{K\times\lambda}{\beta\times\cos\theta} \qquad (1)$$

$$d_{101}[\mathrm{nm}] = \frac{\lambda}{2\times\sin\theta} \qquad (2)$$

where K (= 0.89) is the shape factor, λ (= 0.154 nm) is the X-ray wavelength, β is the line-broadening at half-maximum intensity, and θ is the Bragg angle. The crystallite size of ZnO (101) was calculated from the peak at 36° using Eq. (1). The lattice spacing of t-ZrO_2 (101) plane (d_{101}) changes, when Zn is substituted into the ZrO_2 lattice. It has been reported that the lattice spacing corresponds linearly to the amount of substituted Zn and the solubility limit is 19 at% of ZnO. [22] Thus, using the data below 19 at% of ZnO content from Ref. [22], the amount of substituted Zn (x_s) can be expressed by the following equation:

$$x_s\ [\mathrm{at\%}] = 7\times10^3\times \Delta d_{101}\ [\mathrm{nm}] \qquad (3)$$

where Δd_{101} is the difference in d_{101} between ZrO_2 (Zn-0 in this study) and x_sZnO-ZrO_2 solid solution. Using Eq. (3), x_s of FSP-made particles was estimated.

The ZnO content of the samples was evaluated using an energy-dispersive X-ray fluorescence meter (Rigaku EDXL 300, Cu target, 50 kV, 1 mA). ZnO and ZrO_2 prepared by FSP were mixed to obtain reference samples containing 10 wt%, 20 wt%, and 30 wt% of ZnO. The reference samples were mechanically mixed with an internal standard (10 wt% of Ag_2O, Wako, 99%) in a mortar for 10 min. The mixed samples (100 mg) were formed into pellets (10 mm in diameter and 1 mm in thickness) and then measured by XRF to obtain a calibration curve. Similarly, the FSP-made ZnO-ZrO_2 particles were mixed with 10 wt% of Ag_2O, and the mixtures were pelletized for XRF analysis.

X-ray photoelectron spectroscopy (XPS) was performed using an X-ray photoemission spectrometer (Thermo Fisher Scientific, Nexsa) equipped with monochromatic Al Kα radiation (hv = 1486.68 eV, pass energy = 20 eV). The samples were mounted on an aluminum plate with adhesive carbon tape, and the diameter of the measured spot was 400 μm. To compensate for the eventual surface charging, built-in electron and argon ion neutralizers

were used. The base pressure of the system was below 5×10^{-7} Pa. For the analysis, the background was subtracted using the Shirley method, and the C 1s peak at 284.6 eV was used for charge correction.

N_2 adsorption was performed using a BELSORP-Mini II (MicrotracBEL Corp.). Before the measurements, the samples were degassed at 150 °C under vacuum at < 1 kPa for 1 h. The specific surface area (SSA, $m^2\ g^{-1}$) was calculated from the amount of adsorbed N_2 on the particle surface at -196 °C by the Brunauer–Emmett–Teller (BET) method. The BET-equivalent diameter was calculated using Eq. (4),

$$d_{\mathrm{BET}}\ [\mathrm{nm}] = \frac{6000}{\mathrm{SSA} \times \rho_{\text{t-ZrO2}}} \qquad (4)$$

where $\rho_{\text{t-ZrO2}}$ (= 6.1 g cm^{-3}) is the density of tetragonal ZrO_2. Additionally, the pore-size distribution was obtained using the Barrett–Joyner–Halenda (BJH) method.

The particle morphology and distribution of the Zn and Zr species were investigated using an ultra-high resolution transmission electron microscope (JEOL, JEM–ARM200F) equipped with a spherical aberration corrector for a STEM probe. The sample was dispersed in ethanol, and the suspension was dropped onto a Cu-coated carbon support film (Okenshoji, NP–C15) to deposit the particles on the film. Elemental maps of Zn, Zr, and O were recorded using an energy-dispersive X-ray (EDX) detector.

2.3 Evaluation for catalytic activity

The ZnO-ZrO_2 powders were pressed at 20 MPa, crushed, and sieved to 1.18-1.7 mm. The pelletized samples (0.5 g) were mixed with 1 g of quartz sand (Wako). A mixture of the pelletized powder and quartz sand was placed in a fixed-bed tubular reactor with an inner diameter of 6 mm. A mixture of CO_2: H_2: N_2 (= 1: 3: 1) was introduced into the reactor at 30 $mL_{STP}\ min^{-1}$. The gas pressure was limited by one of the Japanese laws (High Pressure Gas Safety Act, 1.0 MPa or less) and was kept at 1.0 MPa. The catalyst bed temperature was measured using a K-type thermocouple to determine the catalytic activity at 250-350 °C.

The reactant and product concentrations at the reactor outlet were analyzed using an online gas chromatograph (Shimadzu, GC-2014) equipped with flame ionization and thermal conductivity detectors. The CO_2 conversion (X_{CO2}), selectivity to methanol (S_{MeOH}), and yield of methanol (Y_{MeOH}) were determined as follows:

$$X_{CO2}[\%]=\frac{F_{CO2,\,in}-F_{CO2,\,out}}{F_{CO2,\,in}}\times 100 \quad (4)$$

$$S_{MeOH}[\%]=\frac{F_{MeOH,\,out}}{F_{CO,\,out}+F_{MeOH,\,out}}\times 100 \quad (5)$$

$$Y_{MeOH}[\%]=\frac{X_{CO2}\times S_{MeOH}}{100} \quad (6)$$

where $F_{A,\,in}$ and $F_{A,\,out}$ are the flow rates of the A species (mol s^{-1}) at the inlet and the outlet, respectively.

3. Results and Discussion

3.1 Surface area and pore structure of FSP-made ZnO-ZrO_2

Table 1 ZnO content, SSA, and pore volume of the FSP-made particles.

Sample	ZnO/(ZnO+ZrO_2), at%		ZnO/(ZnO+ZrO_2), wt% [c]	SSA $m^2\ g^{-1}$	Total pore volume $cm^3\ g^{-1}$
	Estimated [a]	Measured [b]			
Zn-0	0	N/A	0	208	2.5
Zn-14	14	14	9.6	195	2.3
Zn-28	27	28	20	206	2.6
Zn-40	39	40	30	164	1.5

[a] The ZnO content was calculated based on the concentration of Zn and Zr dissolved in the solvent.
[b] The ZnO content was measured by XRF.
[c] The mass fraction of ZnO was calculated by the atomic fraction of ZnO measured by XRF.

Table 1 lists the ZnO content, SSA, and pore volume of the FSP-made particles. The measured ZnO contents were in agreement with the values estimated from the metal concentration in the precursor solution. Hereafter, the samples are denoted as Zn-*x*, where *x* is the measured ZnO content in at%. The FSP-made particles had large surface areas of 165-206 $m^2\ g^{-1}$, and the BET equivalent diameter of Zn-0 was 4.7 nm. The diameter of the other ZnO-ZrO_2 samples could not be calculated because it was difficult to obtain the exact densities of the materials.

The SSA remained large after heating the particles in Ar at 400°C for 3h (Fig. S1). Other than Zn-40, the total pore volumes of FSP-made particles were comparable. The pore distribution (Fig. S2) of Zn-40 was narrower than that of the others. The SSA of FSP-made catalysts (165-206 $m^2 g^{-1}$) were 1.2~4-fold larger than those of the previously reported ZnO-ZrO_2 catalysts prepared by FSP (63-89 $m^2 g^{-1}$) [37] and other methods (44-139 m^2/g) [18, 20, 21, 23, 24]. In this work, ZnO-ZrO_2 particles were synthesized under a lean-fuel condition. In contrast, ZnO-ZrO_2 particles were prepared under a slightly rich-fuel condition [37]. The lean-fuel condition reduces the particle residence time in the flame, which limits the particle growth. [39] Therefore, the large SSA of FSP-made ZnO-ZrO_2 in this work is attributed to the shorter residence time of particles in the flame compared to that in the literature [37].

3.2 Distribution of Zn species in the lattice and on the surface of ZrO_2

Figure 2(a) shows the PXRD patterns of FSP-made ZnO-ZrO_2. All samples exhibited peaks at 30°, 35°, and 50° (triangles), which were assigned to tetragonal ZrO_2. For all samples, the crystallite size of ZrO_2 was 4-5 nm. The crystallite size of Zn-0 is close to the BET equivalent diameter (4.7 nm) of Zn-0. The dominant crystalline phase was tetragonal, in line with the FSP-made ZrO_2 reported in the literature. [40, 41]

When FSP synthesized only ZnO particles, hexagonal ZnO was formed (Fig. S3). Of note, in the diffraction patterns of the FSP-made ZnO-ZrO_2, no peaks of hexagonal ZnO were detected, regardless of the ZnO content (Fig. 1a). It is expected that the Zn species were present as amorphous particles, a ZnO-ZrO_2 solid solution, and/or small ZnO clusters with the size below the detectable limit of PXRD.

The presence of the ZnO-ZrO_2 solid solution was investigated by the shift of the ZrO_2 (101) peak (Figure 2b). The peak shifted to higher angles for higher ZnO contents. The peak locations of Zn-0 and Zn-40 were 30.10° and 30.21°, respectively. The shift from the peak of Zn-0 to Zn-40 was 0.11°. The shift of Zn-40 (0.11°) was smaller than that of a previously reported 25 at%ZnO-ZrO_2 solid solution (approximately 0.3°) [18]. As the

magnitude of the shift corresponds to the amount of substituted Zn [18, 21, 22], the amount of substituted Zn species in Zn-40 was smaller than that in the solid solution. Therefore, some Zn species in Zn-40 were not substituted with Zr species in ZrO_2, and were located on the surface as amorphous particles and/or small ZnO clusters.

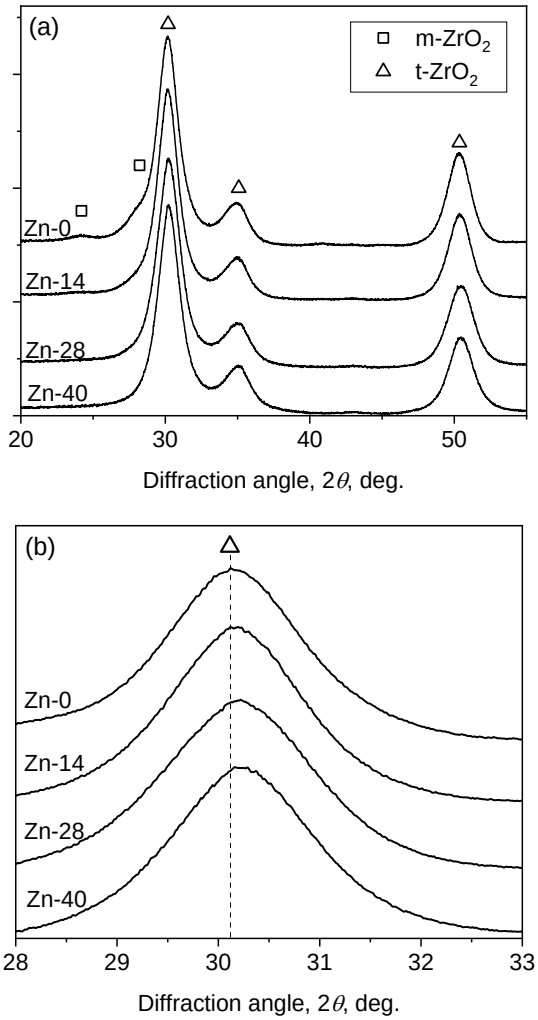

Fig. 2 XRD patterns at 2θ = (a) 20-70° and (b) 28-33° of FSP-made ZnO-ZrO_2.

To explore the presence of amorphous ZnO particles, the samples were treated at 400 °C. Figure 3(a) shows the XRD patterns of FSP-made ZnO-ZrO_2 after heating in Ar at 400 °C for 3 h. A minor fraction of monoclinic ZrO_2 was formed in the Zn-0 sample. Other than Zn-0, the crystalline phase of ZrO_2 remained tetragonal. The crystallite size of all samples was 5 nm, which was comparable to the size before the heat treatment. Hexagonal

ZnO was detected only for Zn-40, and the crystallite size was 16 nm. In other words, Zn species in Zn-14 and Zn-28 remained high dispersion state and/or amorphous.

Furthermore, the absence of a monoclinic phase in the FSP-made ZnO-ZrO_2 implies the substitution of Zn because the Zn substitution leads to the formation of tetragonal ZrO_2. [20, 38]. The presence of the substituted Zn species was confirmed by the shift of the ZrO_2 (101) peak, as shown in Fig. 3(b). Similar to the samples before the heat treatment, the peak shifted to a higher angle in the presence of ZnO, indicating the presence of a solid solution.

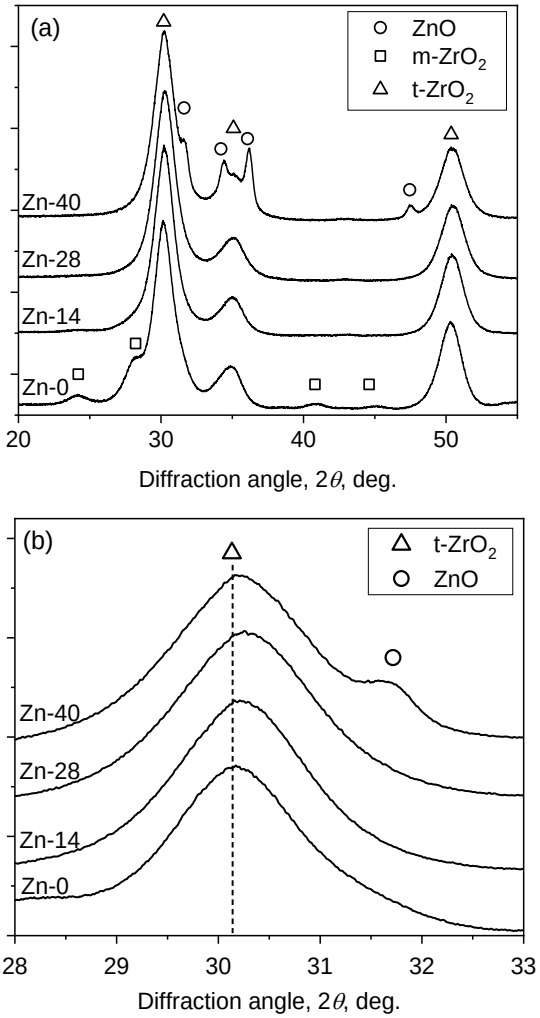

Fig. 3 XRD patterns at 2θ = (a) 20-70° and (b) 28-33° of FSP-made ZnO-ZrO_2 heated in Ar at 400 °C for 3 hours.

The amount of substituted Zn was estimated by the changes in the lattice spacing of t-ZrO_2 (101). Table 2 shows that the lattice spacing (d_{101}) decreased with increasing the ZnO content. The d_{101} also decreased by heating in Ar at 400 °C for 3 hours. Here, we focused on the Δd_{101} value, which is the difference in d_{101} between the pristine Zn-0 (d_{101} = 0.2966 nm) and the corresponding Zn-*x*. The Δd_{101} of Zn-0 after the heating was 0.0002 nm which is the smallest among the catalysts listed in Table 2. Using Δd_{101} and Eq. (3), the amount of substituted Zn (x_s) was estimated. The x_s value tends to increase by increasing the ZnO content. Additionally, the x_s value increased by the heat treatment. The largest x_s was 9 at% for Zn-28 after the heating. The increase of x_s by the heat treatment was caused by the migration of Zn species from the surface into the lattice. Even after the heating, the x_s value of all the samples (Table 2) was smaller than the ZnO content (Table 1). Therefore, some Zn species were located on the surface regardless of the ZnO content.

Table 2 Lattice spacing of ZrO_2 (101) plane (d_{101}), the change in d_{101}, (Δd_{101}), and amount of substituted Zn (x_s)

Sample	Before the heat treatment [a]			After the heat treatment [a]		
	d_{101} [b] [nm]	Δd_{101} [c] [nm]	x_s [d] [at%]	d_{101} [b] [nm]	Δd_{101} [c] [nm]	x_s [d] [at%]
Zn-0	0.2966	0	N/A	0.2964	0.0002	N/A
Zn-14	0.2961	0.0005	3	0.2957	0.0009	6
Zn-28	0.2960	0.0006	4	0.2952	0.0014	9
Zn-40	0.2956	0.0010	7	0.2954	0.0012	8

[a] Particles were heated in Ar at 400 °C for 3 hours.
[b] The lattice spacing of ZrO_2 (101) was calculated by Eq. (2).
[c] The Δd_{101} was calculated by subtracting d_{101} of the sample from that of Zn-0 before the heat treatment (0.2966 nm).
[d] The amount of substituted Zn (x_s) was estimated using Eq. (3).

The above discussions suggested the presence of Zn spices on the surface. When ZnO content was 40 at%, hexagonal ZnO particles were formed by heat treatment. By contrast, the ZnO particles were not observed in Zn-

28; thus, the dispersion state of Zn species on the surface was unclear. Here, the Zn distribution in Zn-28 was explored by microscopic imaging. Figure 4(a, b) shows the STEM images of Zn-28. The particle size was uniform, and the diameter was approximately 5 nm. EDX elemental mapping images (c-f) show that the distributions of Zn and Zr species were identical. Therefore, the Zn species on the surface were uniformly distributed.

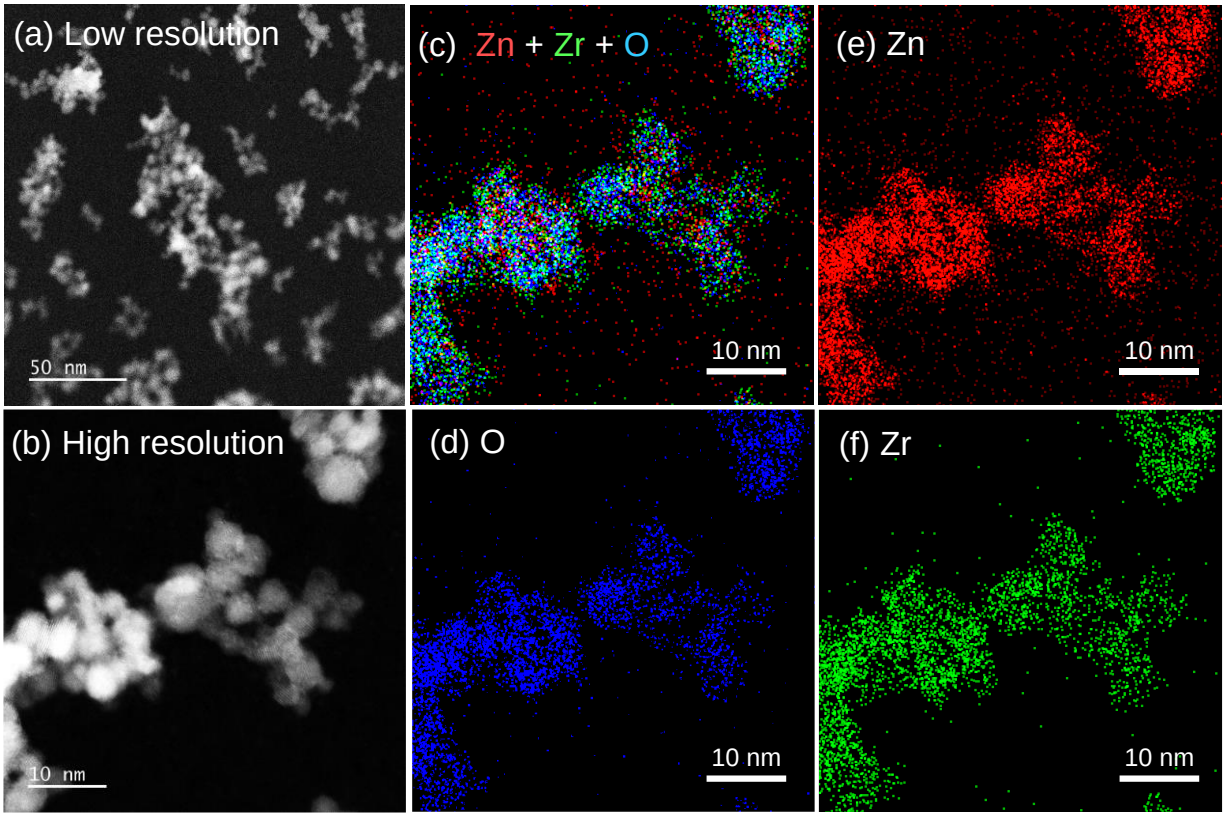

Fig. 4 STEM images (a, b) and EDX mapping (c-f) of Zn-28. More STEM images are shown in Fig. S4.

The oxidation state of the Zn species in the FSP-made ZnO-ZrO_2 was investigated using XPS. Figure 5 shows the Zn 2P XPS spectra of FSP-made ZnO-ZrO_2. The C1s peak at 284.6 eV (Fig. S5) corrected the peak locations of the spectra. For all Zn contents, the Zn $2p_{3/2}$ and Zn $2p_{1/2}$ peaks were observed at 1021.9 and 1044.9 eV, respectively. The peak location indicates the Zn^{2+} state, in line with other flame-made ZnO [42, 43]. In addition, the Zn species in ZnO-ZrO_2 solid solution exhibited the exact peak locations. [21, 22] In the O 1s spectra (Fig.

S6), two peaks were evident at 529.8 and 531.5 eV. The former can be assigned to the lattice oxygen of ZrO_2 and ZnO, while the latter was done to surface hydroxyl groups and oxygen near defective sites. [19, 44, 45]

The ZnO content significantly affected the oxidation state of ZrO_2. Figure 6 shows the Zr 3d XPS spectra of the FSP-made ZnO-ZrO_2. Deconvolution of the spectra revealed four peaks. The two intense peaks at 181.8 eV and 184.2 eV correspond to Zr $3d_{5/2}$ and Zr $3d_{3/2}$ peaks, respectively, indicating the presence of the Zr^{4+} state. [46] Other peaks at 182.9 eV and 185.3 eV possess higher binding energies than those of Zr^{4+}, suggesting the presence of partially reduced $Zr^{\delta+}$ ($\delta < 4$) [47, 48] As shown in Table 3, the peak-area ratio of $Zr^{\delta+}$ to Zr^{4+} increased when the ZnO content increased from 0 to 28 at%. By further increasing the ZnO content from 28 to 40 at%, the ratio declined to a comparable level of Zn-0. Therefore, the $Zr^{\delta+}$ state was prominent below 28 at% of ZnO content in FSP-made ZnO-ZrO_2.

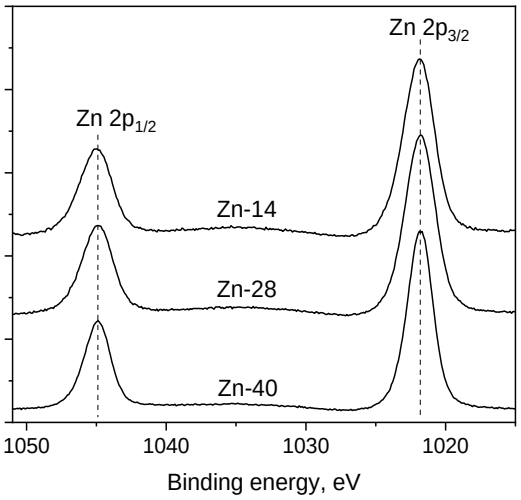

Fig. 5 Zn 2p XPS spectra of FSP-made ZnO-ZrO_2.

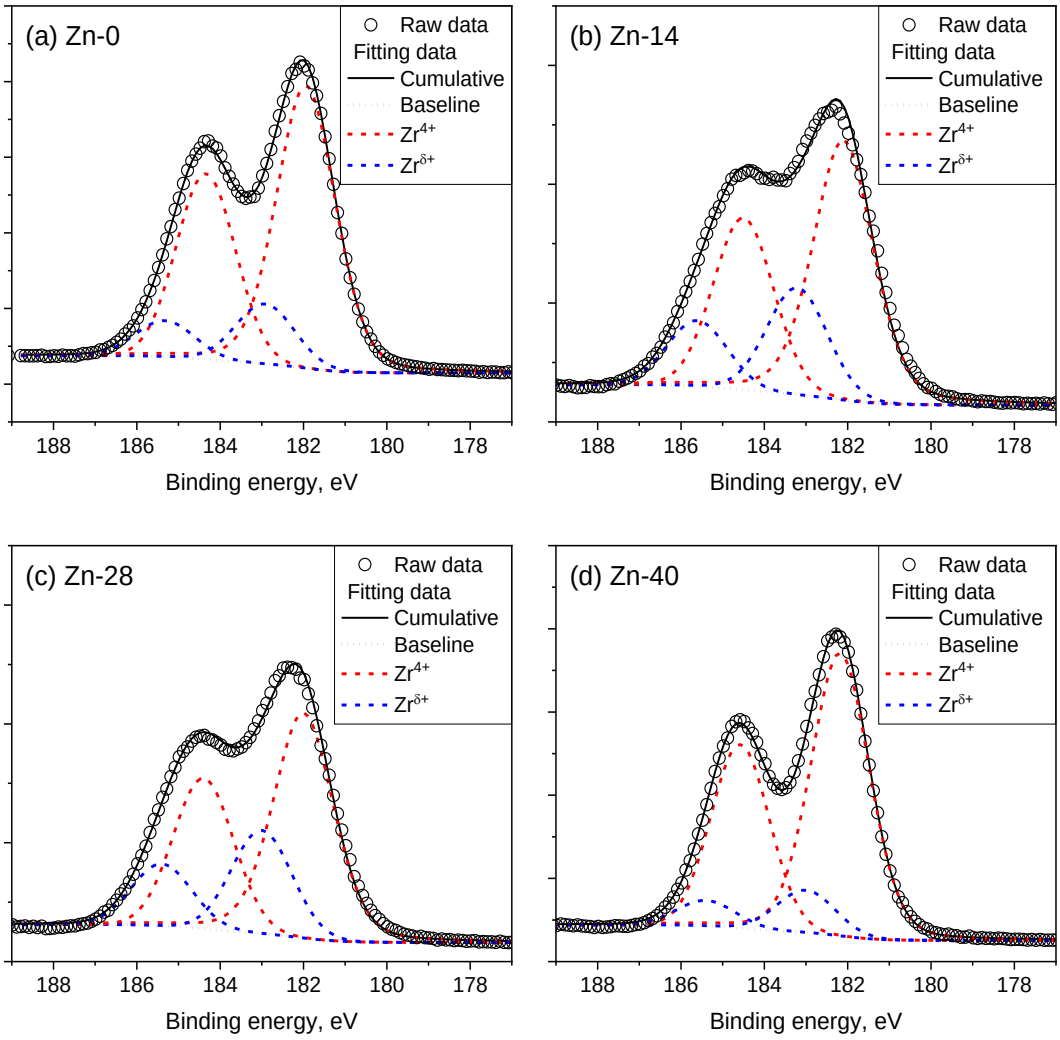

Fig. 6 Zr 3d XPS spectra of FSP-made ZnO-ZrO_2.

Table 3 Peak positions, FWHM and peak-area ratios of deconvoluted Zr^{4+} and $Zr^{\delta+}$ peaks in the Zr $3d_{5/2}$ peak of FSP-made ZnO-ZrO_2.

Sample	Peak position in Zr $3d_{5/2}$, eV[※]		FWHM of Zr^{4+} and $Zr^{\delta+}$ peaks	Peak area ratio of $Zr^{\delta+}/Zr^{4+}$ [†]
	Zr^{4+}	$Zr^{\delta+}$		
Zn-0	181.9	182.9	1.7	0.19
Zn-14	181.8	182.9	1.6	0.37
Zn-28	181.7	182.7	1.7	0.41
Zn-40	181.9	182.7	1.6	0.14

[※] The peak locations of Zr species in Zr $3d_{5/2}$ were set to be 2.4 eV lower than those in Zr $3d_{3/2}$. [47]

[†] The peak-area ratio of Zr $3d_{5/2}$ to Zr $3d_{3/2}$ was fixed at 1.5.

3.3 Catalytic activity of FSP-made ZnO-ZrO_2

According to the literature [18, 19, 21, 22], Zn-O-Zr sites in a ZnO-ZrO_2 solid solution are the active sites for CO_2-to-methanol hydrogenation. It is expected that catalytic activity of Zn-28 and Zn-40 is higher than that of Zn-14, because the amount of the substituted Zn species in Zn-28 and Zn-40 was larger than that in Zn-14 (Table 2). Hence, the performances of Zn-28 and Zn-40 for CO_2 hydrogenation to methanol were evaluated. Figure 7 shows the CO_2 conversion and methanol selectivity of Zn-28 and Zn-40 at various reaction temperatures. The CO_2 conversion of Zn-28 was higher than that of Zn-40. By increasing the temperature, the CO_2 conversion increased, while the selectivity to methanol decreased. For both catalysts, the dominant by-product was CO, and the formation of CH_4 was negligible. The formation of CO at high temperatures is due to the reverse water-gas shift reaction ($CO_2 + H_2 \rightarrow CO + H_2O$), which is thermodynamically favorable at high temperatures. [20, 21] When the methanol selectivity of Zn-28 and Zn-40 was plotted as a function of the conversion, both data lay on an identical interpolated line (Fig. S7), indicating that both catalysts contain the same type of catalytic sites.

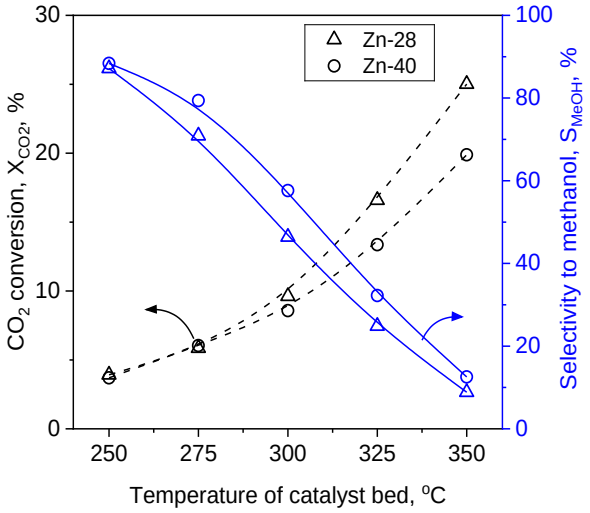

Fig. 7 CO_2 conversion and the methanol selectivity of Zn-28 and Zn-40 for CO_2 hydrogenation to methanol.

The performance of the Zn-28 catalyst and the reported ZnO-ZrO_2 catalysts were summarized in Table 4. According to the literatures, the achievement of high CO_2 conversion (around 9%) needed high reaction

temperatures (330-360 °C). In fact, the CO_2 conversion values were less than 5% at a low reaction temperature (300 °C). Our catalyst, Zn-28, surprisingly showed 9% of CO_2 conversion at 300 °C. As described later, the FSP-made ZnO-ZrO_2 had the larger number of active sites than the ZnO-ZrO_2 prepared by a conventional method, resulting in the high CO_2 conversion even at the low temperature. Because our space velocity (3600 mL_{STP} g^{-1}_{cat} h^{-1}) was very low, it can be natural that Zn-28 showed the high CO_2 conversion. Next, we examined the methanol selectivity. The methanol selectivity tends to increase with elevating the reaction pressure and decreasing CO_2 conversion. In fact, 11.5 at%ZnO-ZrO_2 [19] and ZnO-ZrO_2 (15wt% as Zn) [21] showed the high methanol selectivity (around 80%) when the reaction pressure was high (2.0 MPa) and the CO_2 conversion was low (3-5%). Due to the low pressure (1.0 MPa) and the high CO_2 conversion (9%), the methanol selectivity over Zn-28 (48%) was lower than those of the above two cases. Finally, we focused on the methanol yield. We succeeded that the yield of Zn-28 (4.3%) was comparable with those over ZnO-ZrO_2 (2.5-4.1%) even when our reaction condition was milder: the reaction pressure, limited by one of the Japanese laws, was low (1.0 MPa) and the reaction temperature was also low (300 °C).

It has been reported that Zn-O-Zr sites in the solid solutions are active sites. [18, 19, 21] Although not all the Zn species in Zn-28 were substituted into the ZrO_2 lattice (Table 2), some Zn species were present as Zn-O-Zr sites in a ZnO-ZrO_2 solid solution. In addition, the SSA of Zn-28 (206 m^2 g^{-1}) is significantly larger than the solid solution reported in the literature (44 m^2 g^{-1} [18] and 96 m^2 g^{-1} [21]). Therefore, FSP has a significant advantage as it can form a ZnO-ZrO_2 solid solution with high SSA.

Table 4 Catalytic performance of Zn-28 and ZnO-ZrO_2 catalysts in literature for CO_2 hydrogenation to methanol.

	Temp. [°C]	Pressure [MPa]	F/W [$mL_{STP}/ g^{-1}_{cat} h^{-1}$]	CO_2 conversion [%]	CH_3OH selectivity [%]	CH_3OH yield [%]
28 at%ZnO-ZrO_2 (Zn-28)	300	1.0	3600	9	48	4.3
13 at%ZnO-ZrO_2 [18]*	330	2.0	6000	9	45	4.1
11.5 at%ZnO-ZrO_2 [19]*	300	2.0	24000	3.4	84	2.9
ZnO-ZrO_2 [21]*, † (15 wt% as Zn)	300	2.0	9000	5	75	3.8
	360			9	28	2.5

* Adopted from Fig. S2 [18], Fig. 1 [19] and Fig. 12 [21], respectively.
† The ZrO_2 support was calcinated at 700°C before the impregnation of Zn.

4. Conclusions

In this study, ZnO-ZrO_2 catalysts were prepared using FSP under a lean-fuel condition, and the effect of ZnO content (14, 28, and 40 at%) was investigated. The FSP-made particles had a large surface area (165-206 $m^2 g^{-1}$) regardless of the ZnO content. A fraction of Zn species in FSP-made particles was present as a ZnO-ZrO_2 solid solution, which FSP could not obtain in previous work. FSP-made 28at% ZnO-ZrO_2 catalyst exhibited 9% of the CO_2 conversion and 48% of the selectivity to methanol for CO_2-to-methanol hydrogenation at 300 °C and 1.0 MPa, resulting in the high yield of methanol (4.3%). This excellent activity is attributed to forming of a ZnO-ZrO solid solution with high SSA.

Acknowledgements

This work was supported by Leading Initiative for Excellent Young Researchers (LEADER) of the Ministry of Education, Culture, Sports, Science and Technology (MEXT), Japan. STEM measurements were supported by the microstructural characterization platform at Osaka University (JPMXP09A21OS0012) in a nanotechnology platform project sponsored by MEXT, Japan. XPS measurements were performed at Industrial Technology Institute, Miyagi Prefectural Government.

Conflicts of interest

There are no conflicts of interest to declare.

References

[1] G.A. Olah, Towards oil independence through renewable methanol chemistry, Angew. Chem. Int. Ed., 52 (2013) 104-107.

[2] K. Samson, M. Śliwa, R.P. Socha, K. Góra-Marek, D. Mucha, D. Rutkowska-Zbik, J.F. Paul, M. Ruggiero-Mikołajczyk, R. Grabowski, J. Słoczyński, Influence of ZrO_2 structure and copper electronic state on activity of Cu/ZrO_2 catalysts in methanol synthesis from CO_2, ACS Catal., 4 (2014) 3730-3741.

[3] S. Kattel, B. Yan, Y. Yang, J.G. Chen, P. Liu, Optimizing binding energies of key intermediates for CO_2 hydrogenation to methanol over oxide-supported copper, J. Am. Chem. Soc., 138 (2016) 12440-12450.

[4] T. Witoon, J. Chalorngtham, P. Dumrongbunditkul, M. Chareonpanich, J. Limtrakul, CO_2 hydrogenation to methanol over Cu/ZrO_2 catalysts: Effects of zirconia phases, Chem. Eng. J., 293 (2016) 327-336.

[5] I. Ro, Y. Liu, M.R. Ball, D.H.K. Jackson, J.P. Chada, C. Sener, T.F. Kuech, R.J. Madon, G.W. Huber, J.A. Dumesic, Role of the Cu-ZrO_2 Interfacial Sites for conversion of ethanol to ethyl acetate and synthesis of methanol from CO_2 and H_2, ACS Catal., 6 (2016) 7040-7050.

[6] I.A. Fisher, A.T. Bell, In-situInfrared study of methanol synthesis from H_2/CO_2 over Cu/SiO_2 and $Cu/ZrO_2/SiO_2$, J. Catal., 172 (1997) 222-237.

[7] M. Behrens, F. Studt, I. Kasatkin, S. Kühl, M. Hävecker, F. Abild-Pedersen, S. Zander, F. Girgsdies, P. Kurr, B.-L. Kniep, M. Tovar, R.W. Fischer, J.K. Nørskov, R. Schlögl, The active site of methanol synthesis over $Cu/ZnO/Al_2O_3$ Industrial Catalysts, Science, 336 (2012) 893-897.

[8] J. Graciani, K. Mudiyanselage, F. Xu, A.E. Baber, J. Evans, S.D. Senanayake, D.J. Stacchiola, P. Liu, J. Hrbek, J.F. Sanz, Highly active copper-ceria and copper-ceria-titania catalysts for methanol synthesis from CO_2, Science, 345 (2014) 546-550.

[9] T. Witoon, T. Numpilai, T. Phongamwong, W. Donphai, C. Boonyuen, C. Warakulwit, M. Chareonpanich, J. Limtrakul, Enhanced activity, selectivity and stability of a CuO-ZnO-ZrO_2 catalyst by adding graphene oxide for CO_2 hydrogenation to methanol, Chem. Eng. J., 334 (2018) 1781-1791.

[10] O. Martin, A.J. Martín, C. Mondelli, S. Mitchell, T.F. Segawa, R. Hauert, C. Drouilly, D. Curulla-Ferré, J. Pérez-Ramírez, Indium oxide as a superior catalyst for methanol synthesis by CO_2 hydrogenation, Angew. Chem. Int. Ed., 55 (2016) 6261-6265.

[11] Z. Shi, Q. Tan, D. Wu, A novel Core–Shell structured CuIn@SiO_2 catalyst for CO_2 hydrogenation to methanol, AIChE J., 65 (2019) 1047-1058.

[12] H. Bahruji, M. Bowker, G. Hutchings, N. Dimitratos, P. Wells, E. Gibson, W. Jones, C. Brookes, D. Morgan, G. Lalev, Pd/ZnO catalysts for direct CO_2 hydrogenation to methanol, J. Catal., 343 (2016) 133-146.

[13] N. Iwasa, T. Mayanagi, N. Ogawa, K. Sakata, N. Takezawa, New catalytic functions of Pd–Zn, Pd–Ga, Pd–In, Pt–Zn, Pt–Ga and Pt–In alloys in the conversions of methanol, Catal. Lett., 54 (1998) 119-123.

[14] X. Nie, X. Jiang, H. Wang, W. Luo, M.J. Janik, Y. Chen, X. Guo, C. Song, Mechanistic understanding of alloy effect and water promotion for Pd-Cu bimetallic catalysts in CO_2 hydrogenation to methanol, ACS Catal., 8 (2018) 4873-4892.

[15] F. Studt, I. Sharafutdinov, F. Abild-Pedersen, C.F. Elkjær, J.S. Hummelshøj, S. Dahl, I. Chorkendorff, J.K. Nørskov, Discovery of a Ni-Ga catalyst for carbon dioxide reduction to methanol, Nature Chem., 6 (2014) 320.

[16] S. Tada, S. Satokawa, Effect of Ag loading on CO_2-to-methanol hydrogenation over Ag/CuO/ZrO_2, Catal. Commun., 113 (2018) 41-45.

[17] C. Fröhlich, R.A. Köppel, A. Baiker, M. Kilo, A. Wokaun, Hydrogenation of carbon dioxide over silver promoted copper/zirconia catalysts, Appl. Catal. A-Gen., 106 (1993) 275-293.

[18] J. Wang, G. Li, Z. Li, C. Tang, Z. Feng, H. An, H. Liu, T. Liu, C. Li, A highly selective and stable ZnO-ZrO_2 solid solution catalyst for CO_2 hydrogenation to methanol, Science Advances, 3 (2017) e1701290.

[19] J. Wang, C. Tang, G. Li, Z. Han, Z. Li, H. Liu, F. Cheng, C. Li, High-Performance M_aZrO_x (Ma = Cd, Ga) Solid-Solution Catalysts for CO_2 Hydrogenation to Methanol, ACS Catal., 9 (2019) 10253-10259.

[20] S. Tada, K. Iyoki, Influence of Reaction Temperature on CO_2-to-methanol Hydrogenation over *M*ZrOx (M= Al, Mn, Cu, Zn, Ga, and In), Chem. Lett., 50 (2021) 724-726.

[21] C. Temvuttirojn, Y. Poo-arporn, N. Chanlek, C.K. Cheng, C.C. Chong, J. Limtrakul, T. Witoon, Role of Calcination Temperatures of ZrO_2 Support on Methanol Synthesis from CO_2 Hydrogenation at High Reaction Temperatures over ZnO_x/ZrO_2 Catalysts, Ind. Eng. Chem. Res., 59 (2020) 5525-5535.

[22] S. Tada, N. Ochiai, H. Kinoshita, M. Yoshida, N. Shimada, T. Joutsuka, M. Nishijima, T. Honma, N. Yamauchi, Y. Kobayashi, K. Iyoki, Active Sites on $Zn_xZr_{1-x}O_{2-x}$ Solid Solution Catalysts for CO_2-to-Methanol Hydrogenation, ACS Catal., 12 (2022) 7748-7759.

[23] W. Li, K. Wang, J. Huang, X. Liu, D. Fu, J. Huang, Q. Li, G. Zhan, M_xO_y–ZrO_2 (M = Zn, Co, Cu) Solid Solutions Derived from Schiff Base-Bridged UiO-66 Composites as High-Performance Catalysts for CO_2 Hydrogenation, ACS Appl. Mater. Interfaces, 11 (2019) 33263-33272.

[24] Z. Han, C. Tang, F. Sha, S. Tang, J. Wang, C. Li, CO_2 hydrogenation to methanol on ZnO-ZrO_2 solid solution catalysts with ordered mesoporous structure, J. Catal., 396 (2021) 242-250.

[25] L. Madler, H.K. Kammler, R. Mueller, S.E. Pratsinis, Controlled synthesis of nanostructured particles by flame spray pyrolysis, J. Aerosol Sci, 33 (2002) 369-389.

[26] K. Wegner, B. Schimmoeller, B. Thiebaut, C. Fernandez, T.N. Rao, Pilot plants for industrial nanoparticle production by flame spray pyrolysis, KONA Powder Part. J., 29 (2011) 251-265.

[27] R. Strobel, W.J. Stark, L. Mädler, S.E. Pratsinis, A. Baiker, Flame-made platinum/alumina: structural properties and catalytic behaviour in enantioselective hydrogenation, J. Catal., 213 (2003) 296-304.

[28] W.Y. Teoh, R. Amal, L. Mädler, Flame spray pyrolysis: an enabling technology for nanoparticles design and fabrication, Nanoscale, 2 (2010) 1324-1347.

[29] W.J. Stark, L. Madler, M. Maciejewski, S.E. Pratsinis, A. Baiker, Flame synthesis of nanocrystalline ceria-zirconia: effect of carrier liquid, Chem. Commun., (2003) 588-589.

[30] A. Güntner, N. Pineau, D. Chie, F. Krumeich, S. Pratsinis, Selective sensing of isoprene by Ti-doped ZnO for breath diagnostics, Journal of Materials Chemistry B, 4 (2016) 5358-5366.

[31] K. Fujiwara, S.E. Pratsinis, Single Pd atoms on TiO_2 dominate photocatalytic NO_x removal, Appl. Catal. B-Environ., 226 (2018) 127-134.

[32] A.H. Phakatkar, M.T. Saray, M.G. Rasul, L.V. Sorokina, T.G. Ritter, T. Shokuhfar, R. Shahbazian-Yassar, Ultrafast synthesis of high entropy oxide nanoparticles by flame spray pyrolysis, Langmuir, 37 (2021) 9059-9068.

[33] M. Høj, A.D. Jensen, J.-D. Grunwaldt, Structure of alumina supported vanadia catalysts for oxidative dehydrogenation of propane prepared by flame spray pyrolysis, Appl. Catal. A-Gen., 451 (2013) 207-215.

[34] R. Kydd, W.Y. Teoh, K. Wong, Y. Wang, J. Scott, Q.H. Zeng, A.B. Yu, J. Zou, R. Amal, Flame‐synthesized ceria‐supported copper dimers for preferential oxidation of CO, Adv. Funct. Mater., 19 (2009) 369-377.

[35] K. Fujiwara, S.E. Pratsinis, Atomically dispersed Pd on nanostructured TiO_2 for NO removal by solar light, AIChE J., 63 (2017) 139-146.

[36] S. Ding, H.-A. Chen, O. Mekasuwandumrong, M.J. Hülsey, X. Fu, Q. He, J. Panpranot, C.-M. Yang, N. Yan, High-temperature flame spray pyrolysis induced stabilization of Pt single-atom catalysts, Appl. Catal. B-Environ., 281 (2021) 119471.

[37] P. Šot, G. Noh, I.C. Weber, S.E. Pratsinis, C. Copéret, The Influence of ZnO− ZrO_2 Interface in Hydrogenation of CO_2 to CH_3OH, Helv. Chim. Acta, 105 (2022) e202200007.

[38] G. Štefanić, S. Musić, M. Ivanda, Phase development of the ZrO_2–ZnO system during the thermal treatments of amorphous precursors, J. Mol. Struct., 924-926 (2009) 225-234.

[39] R. Koirala, S.E. Pratsinis, A. Baiker, Synthesis of catalytic materials in flames: opportunities and challenges, Chem. Soc. Rev., 45 (2016) 3053-3068.

[40] R. Mueller, R. Jossen, S.E. Pratsinis, M. Watson, M.K. Akhtar, Zirconia nanoparticles made in spray flames at high production rates, J. Am. Ceram. Soc., 87 (2004) 197-202.

[41] R. Jossen, M.C. Heine, S.E. Pratsinis, M.K. Akhtar, Thermal stability of flame-made zirconia-based mixed oxides, Chem. Vap. Deposition, 12 (2006) 614-619.

[42] C. Ma, X. Zou, A. Li, Z. Gao, L. Luo, S. Shen, J. Zhang, Z. Huang, L. Zhu, Rapid flame synthesis of carbon doped defective ZnO for electrocatalytic CO_2 reduction to syngas, Electrochim. Acta, 411 (2022) 140098.

[43] H. Chen, R. Bo, A. Shrestha, B. Xin, N. Nasiri, J. Zhou, I. Di Bernardo, A. Dodd, M. Saunders, J. Lipton-Duffin, T. White, T. Tsuzuki, A. Tricoli, NiO–ZnO Nanoheterojunction Networks for Room-Temperature Volatile Organic Compounds Sensing, Advanced Optical Materials, 6 (2018) 1800677.

[44] S. Tada, K. Fujiwara, T. Yamamura, M. Nishijima, S. Uchida, R. Kikuchi, Flame spray pyrolysis makes highly loaded Cu nanoparticles on ZrO_2 for CO_2-to-methanol hydrogenation, Chem. Eng. J., 381 (2020) 122750.

[45] R. Al-Gaashani, S. Radiman, A. Daud, N. Tabet, Y. Al-Douri, XPS and optical studies of different morphologies of ZnO nanostructures prepared by microwave methods, Ceram. Int., 39 (2013) 2283-2292.

[46] C. Morant, J. Sanz, L. Galan, L. Soriano, F. Rueda, An XPS study of the interaction of oxygen with zirconium, Surf. Sci., 218 (1989) 331-345.

[47] S. Ardizzone, C.L. Bianchi, XPS characterization of sulphated zirconia catalysts: the role of iron, Surf. Interface Anal., 30 (2000) 77-80.

[48] A.G. Sato, D.P. Volanti, D.M. Meira, S. Damyanova, E. Longo, J.M.C. Bueno, Effect of the ZrO_2 phase on the structure and behavior of supported Cu catalysts for ethanol conversion, J. Catal., 307 (2013) 1-17.